Mon. Not. R. astr. Soc. (1977) **179**, 255–264

Infrared studies of H II regions and dust clouds near K3 – 50

C. G. Wynn-Williams*†, E. E. Becklin†‡, K. Matthews, G. Neugebauer†‡ and M. W. Werner‡ *California Institute of Technology, Pasadena, California 91125, USA*

Received 1976 November 11; in original form 1976 October 19

Summary. New ground-based infrared observations of the K3–50 region are reported at wavelengths between 2 and 34 μm, and at 1 mm. The main results are (a) that the visible nebula K3–50 is displaced from its infrared and radio counterparts, (b) that component C1 (the OH source ON-3) appears very faint at $\lambda \leqslant 20\,\mu$m, and is therefore probably obscured by several hundred magnitudes of visual extinction, (c) that both K3–50 and component C are associated with separate condensations of molecular hydrogen, each of about $3000\,M_{\odot}$, and (d) there are no strong sources in this region at 20 μm other than those associated with H II condensations.

1 Introduction

K3–50 is a small high-excitation optical nebula associated with a group of small H II regions collectively known as W58 (Fig. 1). The most recent major radio continuum study of the area is that of Israel (1976). Two of the compact H II regions have visible counterparts: one of these, called component A at radio wavelengths, lies very close to K3–50 itself while the other is identified with the nebula NGC 6857. The other compact H II regions have no visible counterparts. The question of the extinction in front of the H II regions and of the properties of the neutral material surrounding them has therefore been considered in several studies of the region (e.g. Persson & Frogel 1974). These studies showed that the interstellar component of the extinction is unusually low for a source at this distance (8 kpc), that there are large extinction gradients across the region, and that there are apparent deviations from the normal interstellar reddening law in the material surrounding the K3–50/component A source. Infrared emission associated with K3–50 itself§ was discovered by Neugebauer &

* On leave from Mullard Radio Astronomy Observatory, Cavendish Laboratory, Madingley Road, Cambridge CB3 0HE.

† Guest Observer, Mauna Kea Observatory, Institute of Astronomy, University of Hawaii.

‡ Hale Observatories, California Institute of Technology, Carnegie Institute of Washington.

§ In anticipation of one of the results of this work, namely that there is a positional discrepancy between K3–50 and its infrared counterpart, we will refer to the infrared source as K3–50 IRS throughout the paper.

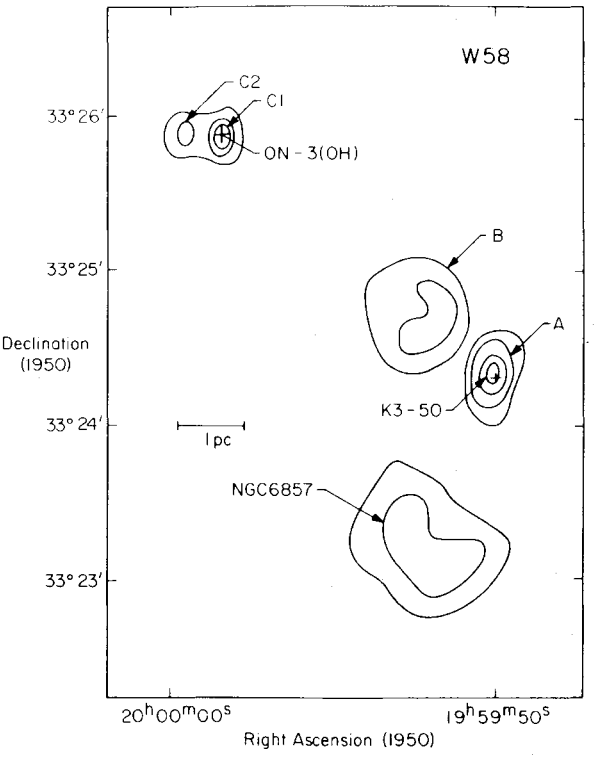

Figure 1. Schematic diagram of the W58 radio sources in the vicinity of K3–50, adapted from Harris (1975) and Israel (1976). The visible nebula K3–50 coincides approximately with radio component A, the OH sources ON-3 coincides with radio component C1. The scale is based on an assumed distance of 8 kpc. In this sketch the contour levels are not evenly spaced.

Garmire (1970) and studied spectrophotometrically by Gillett *et al.* (1975) and Soifer, Russell & Merrill (1976). The other H II regions, including that associated with the maser source ON-3 – designated component C1 by Harris (1975) – have until now received less attention in the published literature.

In this paper we describe an inhomogeneous, but related, set of new infrared observations of the region. These are:

(a) An improved determination of the absolute optical and infrared positions of K3–50 and K3–50 IRS, and a clarification of the relationship between the radio, optical and infrared components of this object.

(b) A determination of the diameter of K3–50 IRS at 10 μm for comparison with the radio size.

(c) An extension of ground-based photometry of K3–50 IRS to 20 and 34 μm.

(d) A search at 20 μm for new infrared sources in the vicinity of, but not coincident with, the radio components.

(e) A search for and study of 2–20-μm emission from component C, which was already known to be unusually weak at infrared wavelengths as compared to most compact H II regions (Wynn-Williams & Becklin 1974).

(f) Observations of the 1-mm continuum emission from the W58 region to determine the distribution of the dust clouds in the vicinity of the H II regions.

This paper should be regarded as complementary to the airborne 30–200-μm study by Thronson & Harper (in preparation) and to the new 15-GHz Cambridge radio synthesis maps (Colley & Scott, in preparation).

2 Results

2.1 VISIBLE AND INFRARED POSITIONS OF K3–50

To obtain a better estimate of the visible position of K3–50, a photograph of the region was taken under conditions of good seeing by F. Schweitzer on the Palomar 1.5-m telescope (Plate 1). It may be seen that the visible object K3–50 is extended on a scale of 1–2 arcsec, particularly towards the east. Because the 1.5-m plate covers too small an area to permit the position of K3–50 to be determined directly from SAO standard stars, a red 48-in Schmidt plate centred on K3–50 was taken by J. Huchra. The positions of a secondary set of 17 standard stars were then measured on the 48-in plate with respect to SAO stars. Corrections for proper motions, typically 0.5 arcsec between 1950 and 1974, were made to the SAO stars. The positions of the point of maximum brightness of K3–50, and of several nearby field stars, were then measured using the 1.5-m plate and the 17 secondary standards. The resultant position of the core of K3–50 is given in Table 1, those of the field stars in Appendix 1. The plates were measured several times; from an examination of the consistency of the results the accuracy of the positions is estimated to be about 0.3 arcsec. This is considerably better than can usually be done from a Palomar Sky Survey plate, especially since K3–50 is located very close to the edge of a standard field.

Table 1. Positions (1950) of sources associated with K3–50. The radio position is from Colley & Scott (in preparation). At 1.65 μm the position of the peak is 1.4 ± 0.5 arcsec south of the 2.2-μm peak.

	h m s	° ′ ″
Visible	19 59 50.01 ± 0.03	33 24 17.4 ± 0.3
2.2 μm	19 59 50.06 ± 0.08	33 24 18.9 ± 1.0
10 μm	19 59 50.11 ± 0.05	33 24 19.4 ± 0.6
Radio	19 59 50.12 ± 0.02	33 24 19.3 ± 0.2

Israel (1976) has published an independent estimate of the position of the optical nebula. His position for K3–50 is about 1.4 arcsec east of ours. Comparison of our Plate 1 with his Fig. 6 indicates that the discrepancy possibly arises as a result of the difference in seeing. Israel's image of K3–50 apparently includes two small field stars about 5 arcsec to the north-east of K3–50, plus the extended nebulosity to the east of the peak.

The position of K3–50 IRS was measured on the Palomar 5-m telescope independently at 10 and 2.2 μm (Table 1). At 10 μm the $f/72$ chopped Gregorian secondary was used, the position of the peak infrared flux being measured with respect to K3–50 and 10 field stars within 30 arcsec seen by a Quantex integrating TV system. The measurements were made on two separate nights, in one case with a 3 arcsec and in one case a 4.5 arcsec diaphragm at 10 μm; no significant difference in position was seen. The 2.2-μm position was measured on three separate nights using the $f/16$ Cassegrain photometer with a focal plane chopper. On each night the position was measured with respect to two or three of the brighter field stars within 30 arcsec of K3–50 using an offset visual eyepiece. Diaphragms ranging in size from 2.5 to 5.0 arcsec were used at 2.2 μm. The errors quoted in Table 1 for the 10- and 2.2-μm positions are based on the consistency of the measurements and on an estimate of the precision with which the visual and infrared diaphragms were lined up with each other. In a separate experiment the position of the peak of the 1.65-μm emission was measured relative to the 2.2-μm position and found to be 1.4 ± 0.5 arcsec south of it. This difference is independent of measurements of field stars and uninfluenced by errors in the visual infrared alignment since exactly the same system (except for filters) is used at both wavelengths.

Fig. 2 shows the positions of the visual object K3–50, and of the 1.65-, 2.2- and 10-μm

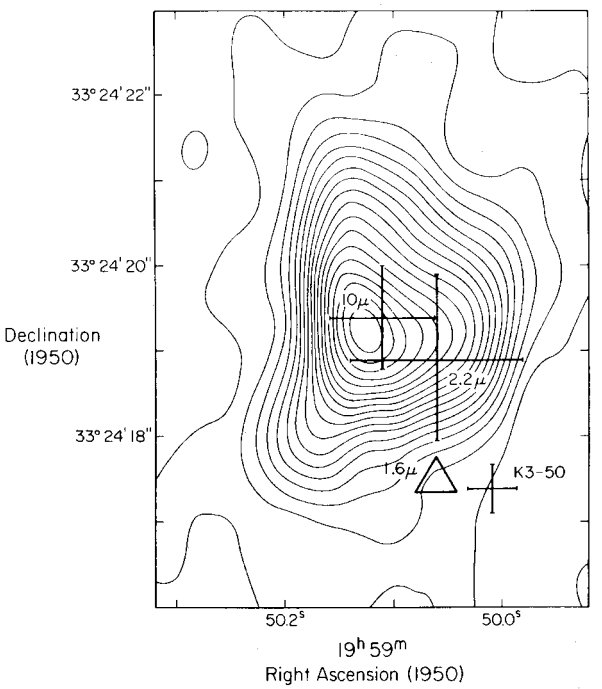

Figure 2. 15-GHz radio map of component A adapted from Colley & Scott (in preparation) with the positions of the visible nebula K3–50, and the 1.65-, 2.2- and 10-μm peaks of K3–50 IRS marked. The 1.65-μm position was measured relative to the 2.2-μm position rather than relative to field stars; error bars have therefore not been drawn at this wavelength.

positions of K3–50 IRS superimposed on the map of the central part of component A at 15 GHz (Colley & Scott, in preparation). It can be seen that the peak of the 10-μm emission, which presumably is from heated dust, coincides very well with the brightest part of the H II region, but that the visible object lies several arcsec away from the peak. The 2.2- and 1.65-μm positions lie between the radio and visual peaks. The most reasonable explanation for this is that the compact H II region is centred on the radio peak, and that there is a very strong extinction gradient across the front of it, so that the apparent position at shorter wavelengths shifts towards regions of lower extinction. Such a situation was predicted by Persson & Frogel (1974) and explains why the extinction as inferred from the long-wavelength data, such as at the 10-μm silicate feature (Gillett *et al.* 1975), is greater than that implied by the short-wavelength measurements. Explanations for the anomalous reddening such as that involving the wavelength dependence of the dust albedo (e.g. Jones 1973; Harris 1975) are therefore unnecessary and would, in any case, have to be modified in the light of the positional discrepancies now found between K3–50 and K3–50 IRS.

Israel (1976) has discussed component A in terms of three almost coincident H II regions having distinct and different physical characteristics. He calls these A1, A2 and A3, having A1 the densest region, associating A2 with the optical nebula, and relating A3 to an envelope seen only at radio wavelengths. We seen no reason to favour such a detailed model over other possible ones and feel that the observations can be equally well explained in terms of a partially ionization-bounded H II region near the edge of an obscuring cloud. A possible geometry is discussed in Section 3.2.

2.2 INFRARED SIZE OF K3–50 IRS

The diameter of K3–50 IRS at wavelengths near 10 μm was determined by making declination scans across it with a narrow slit and comparing the profile thus obtained with profiles

of a star of presumed small dimensions; the method is described by Becklin *et al.* (1973). Data were obtained on two separate nights; in 1974 July, scans were made at 10.1 μm ($\Delta\lambda \approx 5\,\mu$m) and in 1974 October at 12.6 μm ($\Delta\lambda \approx 1\,\mu$m). A 0.7 x 4 arcsec slit was used on both occasions. The comparison stars were IRC +30407 and IRC +40468. The resultant full-width at half maximum of K3–50 IRS, assuming a Gaussian source profile, was 1.2 ± 0.4 arcsec. The 10-μm diameter is therefore significantly smaller than the radio diameter which, based on the same model and Colley & Scott's 15-GHz map, is about 2 arcsec.

2.3 ENERGY DISTRIBUTION OF K3–50 IRS

Fig. 3 shows the energy distribution of K3–50 IRS over the wavelength range 2–34 μm. The interesting new data are the points at 20 and 34 μm which extend the photometry of K3–50 IRS to longer wavelengths. The 34-μm flux density was measured on the 2.2-m telescope at Mauna Kea using a 7-arcsec diaphragm, while the 20-μm point is that measured through a 9-arcsec diaphragm. Also included in Fig. 3 are new photometric measurements made at Mauna Kea with a 9-arcsec diaphragm at wavelengths between 3.4 and 12.5 μm; these data are in good agreement with narrow-band spectrophotometry of Gillett *et al.* (1975) and Soifer *et al.* (1976).

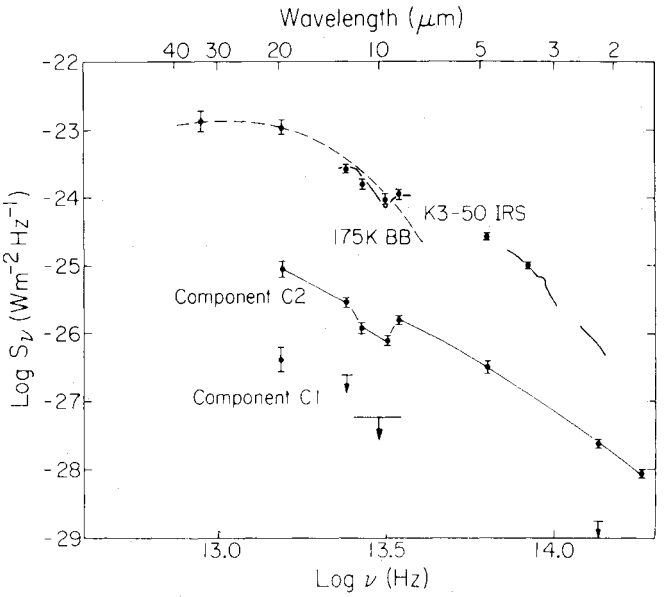

Figure 3. Infrared energy distributions of K3–50 IRS and components C1 and C2. The continuous spectrophotometry is from Gillett *et al.* (1975) from 8 to 13 μm, and Soifer *et al.* (1976) from 2 to 4 μm. The diaphragm sizes are given in Sections 2.3 and 2.5.

The 10–30-μm emission from the central 7–9 arcsec of K3–50 IRS follows approximately a 175 K blackbody curve. Integration of this distribution (including extrapolation to longer wavelengths) leads to a total bolometric luminosity for this region of $4.3 \times 10^5 L_\odot$, based on a distance of 8 kpc. Thronson & Harper (in preparation) measured a total flux from the K3–50 IRS region of $1.7 \times 10^6 L_\odot$ in the 30–1000-μm range, using the C-141 aircraft and a 1-arcmin beam. Their energy distribution peaks at 70 μm, indicating that the dust giving rise to this emission has a temperature of the order of 70 K. Most of the $\lambda >$ 30 μm emission must come from regions exterior to the H II region itself; this is clear from the fact that the 34-μm flux density measured by us with a 7-arcsec beam is only a quarter of that measured at 39 μm with a 1-arcmin beam by Thronson & Harper, and that our total

luminosity for the 7–9 arcsec region of $4.3 \times 10^5 L_\odot$ is only about 20 per cent of the total detected luminosity of $21.3 \times 10^5 L_\odot$.

The luminosity in the form of Lα photons available to heat the grains in the ionized region may be estimated from Colley & Scott's 15-GHz flux density, and is about $1.5 \times 10^5 L_\odot$. This luminosity is significantly less than the infrared luminosities measured with either small or large diaphragms, so there must be additional processes heating the dust. Since the H II region is probably at least partially dust-embedded, absorption of non-ionizing stellar photons, and of nebular photons other than Lα, will almost certainly occur in the neutral matter immediately surrounding the H II region. If the central star is an early main-sequence star the total luminosity available is about 3.5 times the Lα luminosity, namely $5 \times 10^5 L_\odot$ (Panagia 1973); this number could be greater if the exciting star was much larger and cooler than a main-sequence star, or if it had one or more luminous cooler companions. Some of the dust could also be heated as a result of direct absorption of Lyman-continuum photons within the ionized region; the fact that the 10-μm size of K3–50 IRS is smaller than that of the H II region itself provides some support for this picture. Finally, some of the 30–1000-μm luminosity seen in a large diaphragm may well be coming from other sources in the vicinity of K3–50, including component B, NGC 6857 and, perhaps, some hidden dust-embedded non-ionizing stars or protostars.

2.4 SEARCH FOR NEW SOURCES AT 20 μm

A region slightly smaller than Fig. 1 was scanned with a 9-arcsec diaphragm at 20 μm using the Mauna Kea 2.2-m telescope. The actual area mapped was rectangular, bordered by lines at $19^h\,59^m\,49^s$, $20^h\,00^m\,00^s$, $33°\,26'\,26''$ and $33°\,22'\,12''$. The sensitivity was such that a source of 60 Jy (60×10^{-26} W m^{-2} Hz^{-1}) ([20] = –1.9) would have been seen. The only sources seen were K3–50 itself (1100 Jy) and some extended emission near NGC 6857 corresponding to a flux density of order 150 Jy. Components B and C were not seen to the flux density limit of this search. Component C was studied in more detail (Section 2.5) but not component B or NGC 6857, partly because they do not show such interesting radio structure as components A and C.

2.5 COMPONENT C (ON-3)

Harris (1975) showed that component C, which lies about 2 arcmin from K3–50, is a double radio source with two compact components about 15 arcsec apart. The brighter of these, component C1, is identified with a 1720-MHz maser source (Wynn-Williams, Werner & Wilson 1974), and has a compact 1.2-arcsec core at 15 GHz (Colley & Scott).

Because of the known faintness of the sources, infrared measurements were made both by attempting to map a small area around the objects and also by integrating the flux density from the known positions of the H II condensations. These observations showed that component C2 is the more prominent of the two between 2 and 20 μm, although it is still weak as compared with most H II regions. It has a strong silicate absorption feature with about 1.5–2 times the depth of that in K3–50 IRS. The measurements in Fig. 3 were made using a 3.4- or 7.5-arcsec diaphragm, so should include all the emission coming from within the ionized region, which has a diameter of about 2 arcsec (Colley & Scott). The position of maximum 10 μm brightness of object C2 is 1.9 ± 1.5 arcsec north-west of Colley & Scott's radio position: we do not consider this to be a statistically significant discrepancy.

Component C1 is extremely faint at infrared wavelengths. It has been marginally detected only at 20 μm, where the flux density within a 4.5-arcsec diaphragm is only 0.43 ± 0.16 Jy.

Fig. 3 includes limits on the flux density using a 12.5 μm filter 1 μm wide and a broadband (8–13 μm) filter. A flux density of 1.3 ± 0.2 mJy in a 7.5-arcsec diaphragm was actually measured at 2.2 μm from the radio position of object C1 but, since the observation was contaminated by very faint field stars, we have represented this measurement on Fig. 3 as a 3σ upper limit. It is important to emphasize how faint component C1 is, as compared to other compact H II regions. Although its radio flux density is about 10 per cent of that of component A, it is 2500 times fainter than K3–50 IRS at 20 μm.

The flux densities of components C1 and C2 quoted in Fig. 3 were measured with a ≈4-arcsec diaphragm and a 10-arcsec north–south chopper spacing, and with a view to looking specifically for small sources identifiable with the very compact ionized sources. This measurement is, therefore, insensitive to regions of emission with a scale size of 10 arcsec or more. Measurements at 20 μm of a larger region around C1 and C2 were made with a 9-arcsec diaphragm and 18-arcsec chopper spacing at Mauna Kea; extended emission was seen at a peak level of about 30 ± 8 Jy near C2 and 7 ± 2 Jy near C1. These flux densities clearly refer to emission from the neutral material surrounding the compact sources, and are presumably an extrapolation of the 30–200-μm flux attributed by Thronson & Harper to component C. Our sampling was too incomplete, however, to permit integration of the total 20-μm emission from the component C region and relate it to the longer wavelength observations.

2.6 1-mm CONTINUUM OBSERVATIONS

Fig. 4 shows a map of the 1-mm continuum radiation from the K3–50 region. The measurements were made at the prime focus of the Palomar 5-m telescope following the procedure described by Westbrook *et al.* (1976). Emission is seen from two regions, both unresolved by the 1-arcmin beam: one source, with a flux density of 20 ± 4 Jy, coincides within positional uncertainties with K3–50 IRS, while the other, with 15 ± 3 Jy, coincides with component C. Most of the uncertainty results from the calibration. Both these flux densities are considerably greater than the free–free flux densities of the H II regions; the bulk of the emission at this wavelength, therefore, is probably thermal emission from dust, presumably

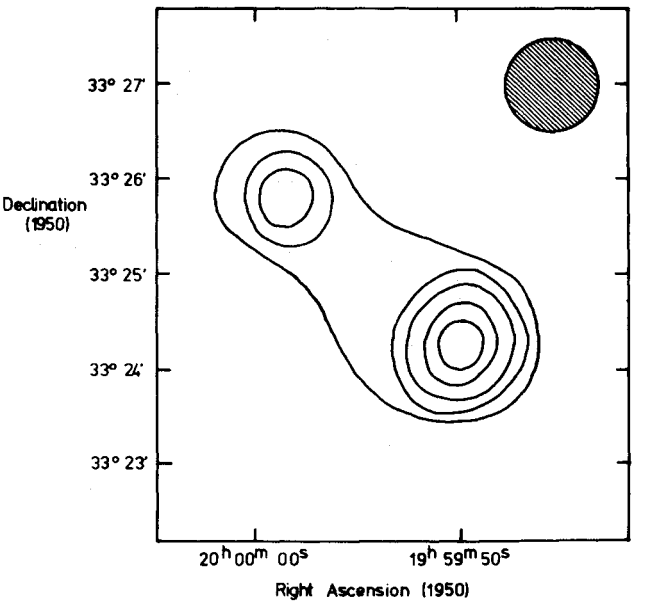

Figure 4. 1 mm continuum emission from the W58 region. Contours are at 4, 8, 12, 16 and 20 Jy per beam area. The shaded circle shows the half-power beam size.

in clouds of molecular hydrogen. The flux densities from the two objects agree with those of Clegg, Rowan-Robinson & Ade (1976).

Westbrook *et al.* (1976) and Scoville & Kwan (1976) have shown that maps of molecular clouds at 1-mm wavelength give, to a first approximation, a good guide to the mass distribution of dust, since the 1-mm emission is relatively insensitive to temperature variations in the cloud. Fig. 4, therefore, indicates that there are two main concentrations of matter in the region under study, one coinciding with K3–50 IRS and one with component C. As shown by Westbrook *et al.* (1976), the column density through the centres of the clouds may be calculated from the 1-mm optical depth. If the cloud angular diameter is about 1 arcmin and the dust temperature 50 K, then the optical depth of either cloud at 1 mm is of the order of 2×10^{-3}. Adopting the same dust parameters as Westbrook *et al.* (1976), a column density of dust of 3×10^{-3} g cm^{-2} is obtained, corresponding to about 90 mag of visual extinction. If a gas-to-dust ratio by mass of 100 is assumed, then the hydrogen column density is 10^{23} molecule cm^{-2}. In a 2-pc diameter spherical cloud (50 arcsec at 8 kpc) such a column density corresponds to a density of 1.6×10^4 molecule cm^{-3} and mass of $3000\,M_\odot$. If the cloud were smaller than 2 pc the density would be larger but the total mass would be the same.

3 Discussion

3.1 THE FAINTNESS OF COMPONENT C1

As discussed in Section 2.6, the ratio of 20-μm to radio flux density is much lower for object C1 than for most other H II regions. We believe that the most likely explanation for component C1's faintness is that it is suffering from significant amounts of extinction at 20 μm, which leads to strong attenuation of both the free–free and dust emission. To estimate this extinction we calculate the minimum emission we expect at 20 μm from within the ionized region. From Fig. 10 of Wynn-Williams & Becklin (1974) it is seen that most compact H II regions have 1–25-μm luminosities about equal to or greater than the luminosity of resonantly trapped Lα radiation. For those regions where this is not true, there is independent evidence in each case, either from the strength of the 10-μm silicate absorption (e.g. Gillett *et al.* 1976; Willner 1976), or from the weakness of the 2-μm emission for large circumnebular or interstellar extinction. In these cases, the correction to the infrared luminosity is such as to place the 1–25-μm luminosity near or above the Lα luminosity. Such a situation is also expected theoretically, even if the dust depletion is as large as 10^3 (e.g. Wright 1973). We will therefore take the unreddened infrared luminosity emitted from within the ionized region to be at least as large as the Lα luminosity as calculated from the radio flux density.

Colley & Scott's map indicates that the radio flux density from an area corresponding to a 4.5-arcsec diaphragm centred on component C1 is 0.6 Jy. The Lα luminosity corresponding to this flux density is $1.5 \times 10^4\,L_\odot$. To calculate the 20-μm flux density it is necessary to assume a colour temperature for the grains in H II regions; in many compact H II regions, including K3–50 IRS (Section 2.3) and the Orion Nebula, the dust associated with the ionized region itself has a colour temperature of about 200 K. If this temperature pertains to component C1, then its 20-μm flux density is at least 35 Jy. Since the measured flux is only 0.43 Jy, the extinction at 20 μm is greater than 4.8 mag. The estimated temperature of the dust depends weakly on the electron density and gas-to-dust ratio in the ionized region (Harwit *et al.* 1972). Over the whole range of 100–400 K, the calculated extinction lies in the narrow range 3.6–4.8 mag at 20 μm.

The extinction at 20 μm therefore appears to be at least 3.6 mag. Extrapolation to the

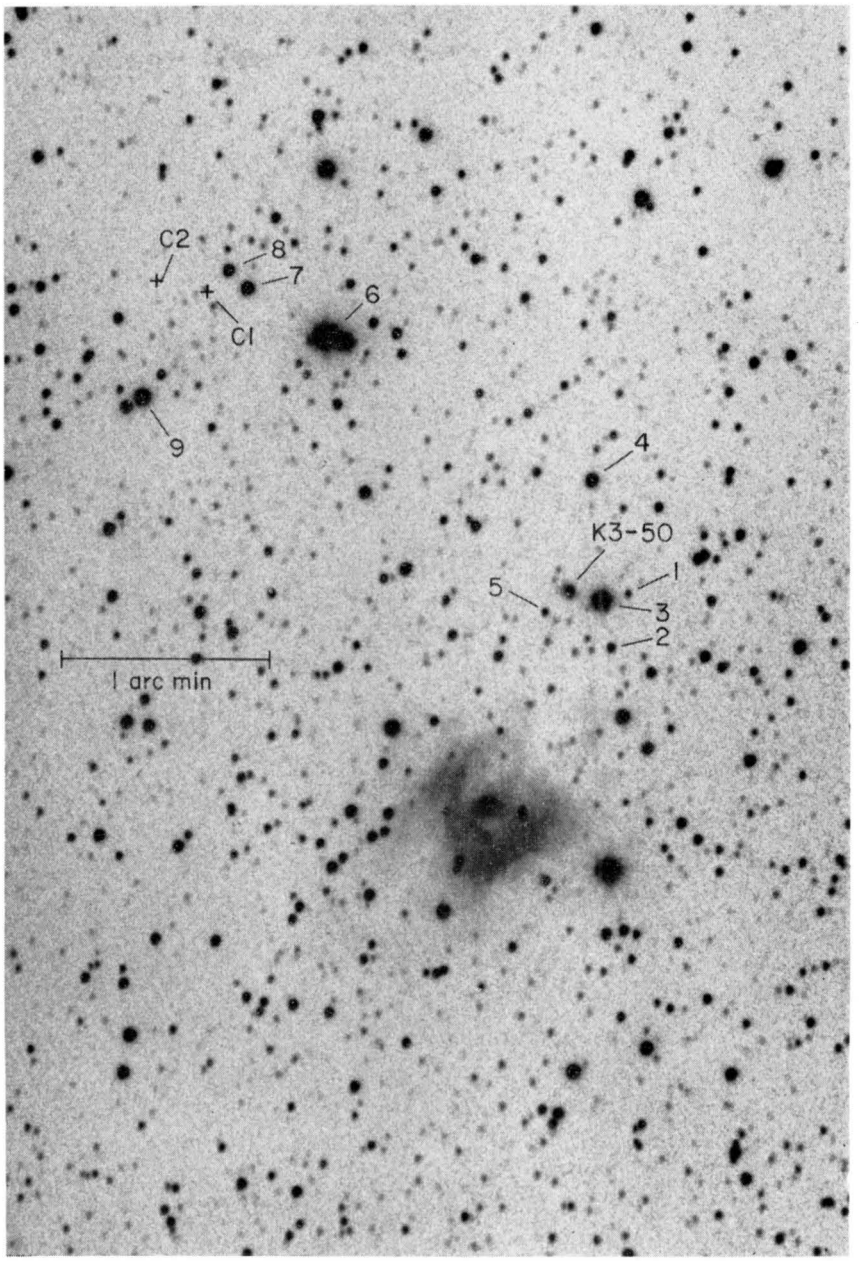

Plate 1. Photograph by F. Schweitzer of the K3−50 region taken with the Palomar 1.5-m telescope, using an 098-04 plate with a GG385 filter, giving a passband of 3900–7000 Å. K3−50 itself, and the location of components C1 and C2, are marked, as are some field stars whose accurate positions are given in Appendix 1.

[*facing page* 262]

visual extinction from the 20-μm extinction is very uncertain, but extending van de Hulst's (1949) curve No. 15 according to a λ^{-1} law leads to a value of $A_v/A_{20\,\mu m}$ of about 100. We therefore deduce that there are several hundred magnitudes of visual extinction towards component C1. This value is, of course, extremely high compared to most other measured H II regions, especially for an object associated with a couple of visible nebulae; the corresponding column density (10^{23}–10^{24} molecule cm^{-2}), however, is about the same order of magnitude as that determined at 1 mm for the molecular cloud. A potentially reliable way of estimating the extinction towards C1 would be to measure the strength of an infrared hydrogen recombination line, such as Brackett-α. The flux predicted for this line is based on the radio free–free flux density, not on the grain properties, and so is subject to many fewer uncertainties than the method used here.

3.2 THE RELATIONSHIP BETWEEN THE COMPACT H II REGIONS AND THE MOLECULAR CLOUDS IN W58

Comparison of the 1-mm map with the radio and infrared data suggest that components A, B and NGC 6857 are associated with one molecular cloud, while C1 and C2 are associated with another. The bright optical nebula NGC 6857 is presumably at the front of its molecular cloud while B, C1 and C2 are either deep within or behind thick layers of dust. Component A is most probably a compact H II region eating its way into the western edge of the molecular cloud; such a configuration would explain the variation of extinction across the source as well as the fact that the radio emission falls off more steeply on the eastern than on the western side of the source. It is possible that some or all of the visible K3–50 nebulosity arises by scattering of nebular radiation from component A by dust grains; this hypothesis could be tested by looking for optical polarization in K3–50.

The configuration we propose for K3–50, namely an H II region eating into the edge of a molecular cloud is very like that proposed for the Orion Nebula H II region and cloud by Zuckerman (1973), Balick, Gammon & Hjellming (1974) and others, but viewed from the side. The question of the frequency with which compact H II regions are found on the edge of, rather than inside, molecular clouds is an interesting one which merits further study, although beset by selection effects.

4 Conclusions

(1) The visible nebula K3–50 and its associated infrared source K3–50 IRS are displaced from each other. At 10 μm the emission coincides with the radio source, but at shorter wavelengths it appears to be displaced to one side as the result of extinction gradients in front of the object.

(2) About a fifth of the total infrared luminosity from a 1-arcmin region centred on K3–50 IRS can be attributed to emission from within the ionized region; the rest comes from outside it.

(3) There are no strong sources within the K3–50 region at 20 μm other than those associated with H II regions.

(4) K3–50 and component C each coincide with a 1-mm continuum emission peak, indicating that each is associated with a molecular cloud. The masses of these clouds are some 3000 $M_\odot$ each.

(5) Component C1 (ON-3) suffers at least 3.6 mag of extinction at 20 μm, and therefore must be behind a molecular cloud of several hundred magnitudes of visual extinction.

(6) The extreme variations in extinction in the region may indicate that some of the compact H II regions are located at the edges of the molecular clouds.

Acknowledgments

We thank the University of Hawaii for observing time on their 2.2-m telescope. We are indebted to our night assistants Frank Cheigh and Peter Hendricks at Mauna Kea, and Gary Tuton at Palomar for help with the observations, to François Schweitzer and John Huchra for taking plates of the region for us, and to Harley Thronson, Al Harper, David Colley and Paul Scott for communicating and allowing us to quote their results prior to publication. This work was performed under NASA grant NGL05-02-207 and NSF grant MPS74-18555A01.

References

Balick, B., Gammon, R. H. & Hjellming, R. M., 1974. *Publ. astr. Soc. Pacific,* **86,** 616.
Becklin, E. E., Matthews, K., Neugebauer, G. & Wynn-Williams, C. G., 1973. *Astrophys. J. Lett.,* **186,** L69.
Clegg, P. E., Rowan-Robinson, M. & Ade, P. A. R., 1976. *Astr. J.,* **81,** 399.
Gillett, F. C., Forrest, W. J., Merrill, K. M., Capps, R. W. & Soifer, B. T.,1975. *Astrophys. J.,* **200,** 609.
Harris, C. S., 1975. *Mon. Not. R. astr. Soc.,* **170,** 139.
Harwit, M., Soifer, B. T., Houck, J. R. & Pipher, J. L., 1972. *Nature Phys. Sci.,* **236,** 103.
Israel, F. P., 1976. *Astr. Astrophys.,* **48,** 193.
Jones, T. W., 1973. *Publ. astr. Soc. Pacific,* **85,** 811.
Neugebauer, G. & Garmire, G., 1970. *Astrophys. J. Lett.,* **161,** L91.
Panagia, N., 1973. *Astr. J.,* **78,** 929.
Persson, S. E. & Frogel, J. A., 1974. *Astrophys. J.,* **188,** 523.
Scoville, N. Z. & Kwan, J., 1976. *Astrophys. J.,* **206,** 718.
Soifer, B. T., Russell, R. W. & Merrill, K. M., 1976. *Astrophys. J.,* **210,** 334
van de Hulst, H. C., 1949. *Rech. Astr. Obs. Utrecht,* **11,** pt 2.
Westbrook, W. E., Werner, M. W., Elias, J. H., Gezari, D. Y., Hauser, M. G., Lo, K. Y. & Neugebauer, G., 1976. *Astrophys. J.,* **209,** 94.
Willner, S. P., 1976. *Astrophys. J.,* **206,** 728.
Wright, E. L., 1973. *Astrophys. J.,* **185,** 569.
Wynn-Williams, C. G. & Becklin, E. E., 1974. *Publ. astr. Soc. Pacific,* **86,** 5.
Wynn-Williams, C. G., Werner, M. W. & Wilson, W. J., 1974. *Astrophys. J.,* **187,** 41.
Zuckerman, B., 1973. *Astrophys. J.,* **183,** 863.

Appendix 1

Field stars in the vicinity of K3−50 and ON-3 (Fig. 1). The errors are about ±0.3 arcsec.

Number	α (1950)			δ (1950)		
	h	m	s	°	′	″
1	19	59	48.63	33	24	16.5
2	19	59	49.06	33	24	00.4
3	19	59	49.26	33	24	14.5
4	19	59	49.45	33	24	50.9
5	19	59	50.61	33	24	11.3
6	19	59	55.71	33	25	35.4
7	19	59	57.58	33	25	50.5
8	19	59	58.02	33	25	56.0
9	20	00	00.13	33	25	18.2